STRUCTURAL BIOLOGY COMMUNICATIONS

ISSN 2053-230X

Cryoannealing-induced space-group transition of crystals of the carbonic anhydrase psCA3

Melissa A. Pinard,[a]‡ Justin J. Kurian,[a]‡ Mayank Aggarwal,[b] Mavis Agbandje-McKenna[a] and Robert McKenna[a]*

[a]Department of Biochemistry and Molecular Biology, University of Florida College of Medicine, 1200 Newell Drive, PO Box 100245, Gainesville, FL 32610, USA, and [b]Division of Biology and Soft Matter, Oak Ridge National Laboratory, Oak Ridge, TN 37831, USA. *Correspondence e-mail: rmckenna@ufl.edu

Received 26 April 2016
Accepted 8 June 2016

Edited by J. Newman, Bio21 Collaborative Crystallisation Centre, Australia

‡ These authors contributed equally to this work.

Keywords: β-carbonic anhydrase; *Pseudomonas aeruginosa*; cryoannealing; crystal packing.

PDB reference: psCA3, 5jj8

Supporting information: this article has supporting information at journals.iucr.org/f

Cryoannealing has been demonstrated to improve the diffraction quality and resolution of crystals of the β-carbonic anhydrase psCA3 concomitant with a change in space group. After initial flash-cooling in a liquid-nitrogen cryostream an X-ray diffraction data set from a psCA3 crystal was indexed in space group $P2_12_12$ and was scaled to 2.6 Å resolution, but subsequent cryoannealing studies revealed induced protein rearrangements in the crystal contacts, which transformed the space group to $I222$, with a corresponding improvement of 0.7 Å in resolution. Although the change in diffraction resolution was significant, only minor changes in the psCA3 structure, which retained its catalytic 'open' conformation, were observed. These findings demonstrate that cryoannealing can be successfully utilized to induce higher diffraction-quality crystals while maintaining enzymatically relevant conformations and may be useful as an experimental tool for structural studies of other enzymes where the initial diffraction quality is poor.

1. Introduction

The packing and geometry of protein crystals are controlled by interrelated variables such as pH, ionic strength, temperature, salt concentration *etc.* which modulate the attractive and repulsive forces that are responsible for the interaction of protein molecules in the crystal lattice. Crystal contacts are often misinterpreted as physiological protein–protein interactions existing in multimeric (such as dimers and dimers of dimers) proteins; however, these contacts are sometimes solely the interactions observed between protein molecules in the unit cell or with molecules in the neighboring unit cell (Krissinel & Henrick, 2007). Additionally, the area of the protein surface patch involved in crystal contacts is normally smaller than those that may be involved in functional contacts. It has been suggested that most of these crystal contacts are formed at random as the crystal grows and the protein is removed from contact with solvent (Pellicane *et al.*, 2008).

To prevent radiation damage, it is now common practice to cryocool protein crystals with liquid nitrogen (either in a pool of liquid nitrogen or in a stream of cold nitrogen) after the addition of a cryoprotectant and prior to data collection (Cosier & Glazer, 1986; Hope, 1988). Cryoannealing is the re-equilibration to room temperature (RT) of a flash-cooled crystal before flash-cooling it again (Yeh & Hol, 1998). As described in previous work (Hanson *et al.*, 2003; Juers & Matthews, 2004; Harp *et al.*, 1998; Kriminski *et al.*, 2002), this

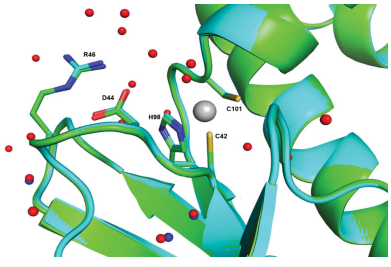

approach has been shown to be beneficial as a procedure for improving diffraction and reducing crystal mosaicity. The initial cryocooling of a crystal can damage or modify the state of the protein-molecule interactions in the crystal lattice; however, submitting the crystal to one or more heating/cooling cycles can help it to recover from some of the deleterious effects of the initial cooling event (Harp *et al.*, 1998).

Carbonic anhydrases (CAs; EC 4.2.1.1) are a family (classes α, β, γ, δ and ζ) of mostly zinc metalloenzymes that catalyze the reversible hydration/dehydration of carbon dioxide/bicarbonate (Frost & McKenna, 2013; Tripp *et al.*, 2001). The β-class CAs (β-CAs) are found in prokaryotes, plants, algae and some animals, with the active-site zinc coordinated by two cysteines, a histidine and an exchangeable zinc-bound solvent (ZBS; Lotlikar *et al.*, 2013; Joseph *et al.*, 2010; Covarrubias, Larsson *et al.*, 2005). In the 'open' active site, an arginine stabilizes an aspartate through a salt-bridge interaction (forming an Asp–Arg dyad), allowing the active-site zinc to be solvent-accessible (Cronk *et al.*, 2001, 2006; Covarrubias, Bergfors *et al.*, 2005; Covarrubias, Larsson *et al.*, 2005).

Pseudomonas aeruginosa, a Gram-negative facultative aerobe, is an opportunistic human pathogen that causes life-threatening chronic infections and nosocomial infections in cystic fibrosis and endocarditis patients (Stover *et al.*, 2000; Oliver *et al.*, 2000; Reyes & Lerner, 1983). This pathogen expresses three β-class CAs (psCA1–psCA3) that have gained interest as possible drug targets in the development of antibacterial agents (Lotlikar *et al.*, 2013).

In this paper, we describe the cryoannealing-induced space-group transition of psCA3 crystals from $P2_12_12$ to $I222$ and the subsequent improved diffraction resolution and structure determination. The determination of the $I222$ crystal structure and its biological implications have been described elsewhere (Pinard *et al.*, 2015).

2. Materials and methods

2.1. Expression and purification of psCA3

The cloning, expression and purification of psCA3 were carried out as described previously (Lotlikar *et al.*, 2013). The recombinant gene was expressed in *Escherichia coli* BL21 (DE3) cells with a His tag and protein expression was induced by the addition of IPTG to a final concentration of 1 m*M* in the presence of 0.5 m*M* $ZnSO_4$. The cells were then harvested, resuspended and lysed as described previously (Pinard *et al.*, 2013). The psCA3 lysate was purified using a nickel column. Nonspecific proteins were washed off the column using 20 m*M* Tris–HCl pH 7.9, 60 m*M* imidazole, 150 m*M* NaCl buffer. The psCA3 protein was eluted with the same buffer but with 300 m*M* imidazole. To confirm the purity of the psCA3, the eluted fractions were run on an SDS–PAGE and stained with Coomassie Blue. Fractions containing psCA3 were pooled and dialyzed against 20 m*M* Tris–HCl pH 7.9, 150 m*M* imidazole, 100 m*M* NaCl, 10% glycerol for 2 h and then against 20 m*M* Tris–HCl pH 7.9, 50 m*M* imidazole, 50 m*M* NaCl, 5% glycerol for 1 h. Finally, psCA3 was dialyzed against 20 m*M* Tris–HCl pH 8.3 three times. The protein was then concentrated to $\sim$10 mg ml^{-1} using an Amicon 10 kDa filter (Millipore, Billerica, Massachusetts, USA).

Table 1
Crystallographic data-collection and refinement statistics for psCA3 in space groups $P2_12_12$ and $I222$.

Values in parentheses are for the highest resolution bin.

PDB code	5jj8	4rxy†
Space group	$P2_12_12$	$I222$
Crystal-to-detector distance (mm)	150	150
Wavelength (Å)	0.917	0.917
Temperature (K)	100	100
Unit-cell parameters (Å)	a = 88.4, b = 69.4, c = 77.7	a = 71.2, b = 77.9, c = 87.7
Resolution (Å)	2.60 (2.64–2.60)	1.90 (1.97–1.90)
Total No. of reflections	44987	49728
No. of individual reflections	14242	16312
Multiplicity	3.2 (2.5)	4.3
Completeness (%)	92.2 (80.0)	98.2 (99.8)
$\langle I/\sigma(I)\rangle$	17.3 (4.5)	14.3 (2.94)
$R_{\rm merge}$‡ (%)	15.3 (38.1)	8.0 (52.6)
$R_{\rm cryst}$§/$R_{\rm free}$¶	0.212/0.275	0.167/0.199
R.m.s.d., bond lengths (Å)	0.009	0.008
R.m.s.d., bond angles (°)	1.240	1.040
Average B factors (Å^2)		
Main chain	50.4	30.9
Side chain	53.2	36.3
No. of protein atoms	3392	1696
No. of water molecules	22	72
Ramachandran statistics (%)		
Favored	93.5	98.1
Allowed	6.5	1.9

† Statistics for PDB entry 4rxy are shown as originally published in Pinard *et al.* (2015). ‡ $R_{\rm merge} = \sum_{hkl}\sum_i |I_i(hkl) - \langle I(hkl)\rangle|/\sum_{hkl}\sum_i I_i(hkl)$. § $R_{\rm cryst} = \sum_{hkl}||F_{\rm obs}| - |F_{\rm calc}||/\sum_{hkl}|F_{\rm obs}|$. ¶ $R_{\rm free} = \sum_{hkl}||F_{\rm obs}| - |F_{\rm calc}||/\sum_{hkl}|F_{\rm obs}|$ for the 5% of collected reflection data that was omitted during refinement.

2.2. Crystallization

Initial crystallization screening of psCA3 was performed in 96-well Intelli-Plate sitting-drop vapor-diffusion crystallization plates using a Gryphon robot (Art Robbins Instruments, Sunnyvale, California, USA). Crystal Screen 2, PEG/Ion and PEG/Ion 2 from Hampton Research, an in-house sodium citrate screen (screening conditions varied from 1.1 to 1.8 *M* sodium citrate, Tris–HCl pH 7.1–8.1) and an in-house ammonium sulfate screen (screening conditions varied from 1.8 to 2.8 *M* ammonium sulfate, 0.1 *M* malic acid, 0.1 *M* imidazole pH 7.0–8.5) prepared using a Rigaku Alchemist DT liquid-handling system were used.

The psCA3 crystals used were obtained from a precipitant consisting of 2.2 *M* ammonium sulfate, 0.1 *M* malic acid, 0.1 *M* imidazole pH 7.5. 0.5 µl drops were prepared by mixing protein solution at $\sim$10 mg ml^{-1} and precipitant solution in a 1:1 ratio and were equilibrated at 290 K against a 60 µl reservoir containing precipitant solution.

2.3. Data collection, indexing and processing

Diffraction data for the $P2_12_12$ crystal form were collected at the F1 station at Cornell High Energy Synchrotron Source (CHESS F1; λ = 0.9177 Å) on an ADSC Q270 detector using a microfocused beam. Data were collected with a crystal-to-

detector distance of 150 mm and a 0.5° oscillation angle with an exposure time of 20 s per image over 110 frames. The data for the *I*222 crystal form of psCA3 were collected as described previously (Pinard *et al.*, 2015). Both crystal forms were indexed and processed using *HKL*-2000 (Otwinowski & Minor, 1997).

2.4. Structure solution and refinement

The initial phases of the $P2_12_12$ form were calculated using the previously solved *I*222 psCA3 structure described in Pinard *et al.* (2015), with water molecules deleted, as a template (PDB entry 4rxy) using the molecular-replacement algorithm in the *PHENIX* suite of programs (Adams *et al.*, 2010). To avoid phase bias, both the zinc ion and the active-site Asp–Arg loop were also deleted from the phasing model.

The graphics program *Coot* (Emsley *et al.*, 2010) was used to view electron-density maps and the psCA3 structure was manually adjusted. Refinement was continued until the R_{work} and R_{free} converged, and the geometry of the final psCA3 model was verified using *MolProbity* (Chen *et al.*, 2010). The data-collection and refinement statistics for the $P2_12_12$ form are summarized in Table 1.

3. Results and discussion

During data collection at the F1 station at CHESS, various psCA3 crystals were screened for diffraction quality; these crystals were pre-soaked with 20% glycerol for various time intervals (1–30 s) and then flash-cooled to 100 K in a nitrogen cryostream. The quality of diffraction (based on the resolution of diffraction and the visual mosaic spread) varied, but the diffraction quality of several crystals was adequate for data collection. Hence, a data set was collected to 2.6 Å resolution and was indexed (χ^2 errors of 0.68 and 13.04% for $P2_12_12$ and *I*222, respectively) in space group $P2_12_12$ (Table 1). After several more crystals were flash-cooled and initial diffraction images were collected, it was decided to try to cryo-reanneal the crystals. Upon several (more than three) heating/cooling cycles it was visually noted that the diffraction resolution and mosaic spread were substantially improved and a data set was collected. These data were subsequently indexed (χ^2 errors of 19.68 and 0.25% for $P2_12_12$ and *I*222, respectively) in space group *I*222 and scaled to 1.9 Å resolution (Table 2). It was concluded that during the cryoannealing process the crystal had undergone an induced space-group transition. The psCA3 *I*222 crystal structure was determined and the biological implications have been described elsewhere (Pinard *et al.*, 2015). Here, we take a 'with hindsight' view of the conformational movements that occur within the psCA3 crystal lattice during the $P2_12_12$ to *I*222 space-group transition.

Table 2
Indexing-error statistics in space groups $P2_12_12$ and *I*222.

	χ^2 error (%)	
Data set	Primitive orthorhombic lattice ($P2_12_12$)	*I*-centered lattice (*I*222)
$P2_12_12$	0.68	13.04
*I*222	19.68	0.25

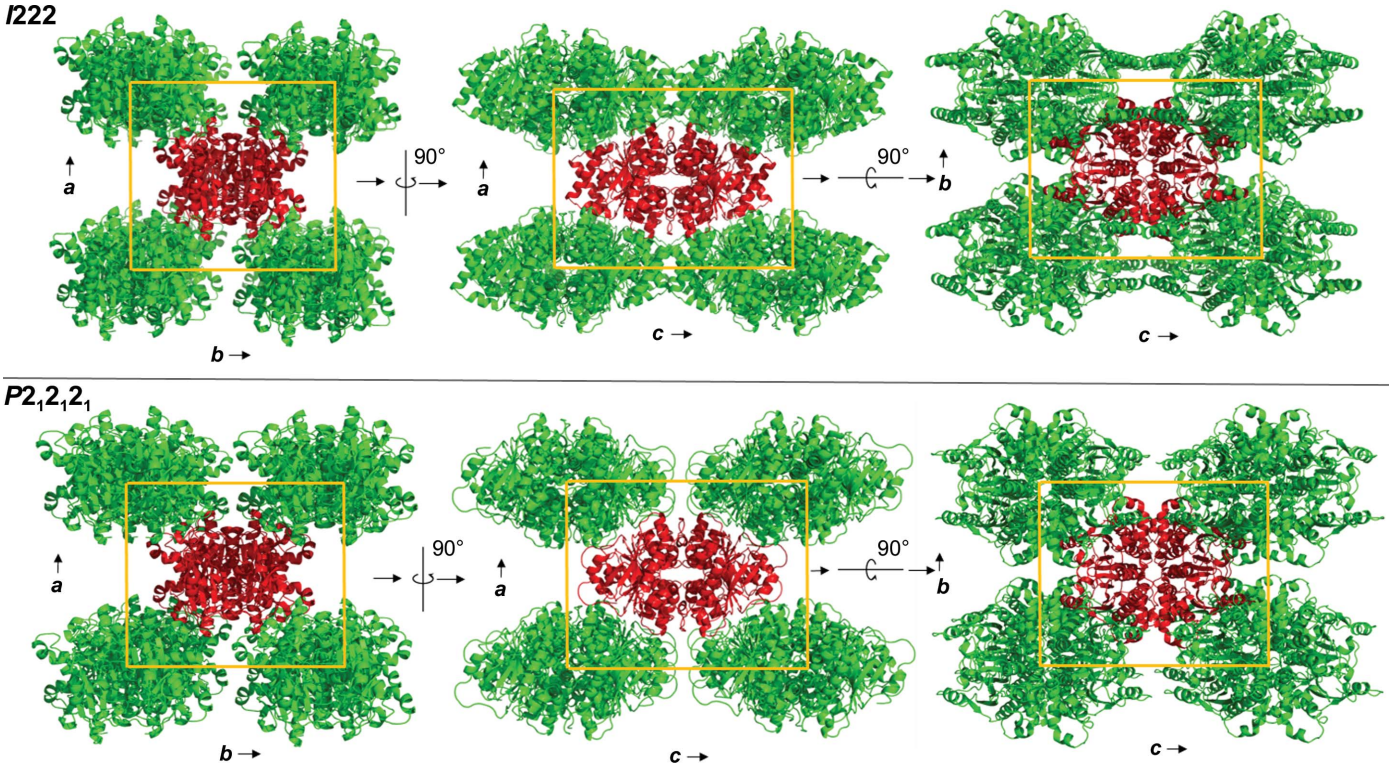

Figure 1
Packing diagram of psCA3 in space groups $P2_12_12$ and *I*222, shown along the *a*–*b*, *a*–*c* and *b*–*c* axes. Unit-cell dimensions are denoted by a yellow box.

Table 3
Crystal-packing information for psCA3 in the orthorhombic space groups *I*222 and $P2_12_12$.

Space group	*I*222	$P2_12_12$
Resolution (Å)	1.9	2.6
Unit-cell parameters (Å)	a = 71.2, b = 77.9, c = 87.7	a = 88.4, b = 69.4, c = 77.7
V_M (Å^3 Da^{-1})	2.51	2.49
No. of molecules in asymmetric unit	1	2
No. of molecules in unit cell	8	8
Symmetry operators (A and B are chain identifiers)	(1) x, y, z (2) x, $-y$, $-z$ (3) $-x$, y, $-z$ (4) $-x$, $-y$, z (5) 1/2 + x, 1/2 + y, 1/2 + z (6) 1/2 + x, 1/2 − y, 1/2 − z (7) 1/2 − x, 1/2 + y, 1/2 − z (8) 1/2 − x, 1/2 − y, 1/2 + z	(1A,B) x, y, z (2A,B) 1/2 + x, 1/2 − y, $-z$ (3A,B) 1/2 − x, 1/2 + y, $-z$ (4A,B) $-x$, $-y$, z
Unit-cell volume (Å^3)	486000	477000

3.1. *I*222 and $P2_12_12$ crystal-packing analysis

The structure of the *I*222 crystal form has been described in Pinard *et al.* (2015) and only the relevant details are included in this study. The structure contained one psCA3 molecule in its asymmetric unit, with eight molecules in the unit cell, with the biological dimer being present (Table 3, Fig. 1). The interactive web server application *PDBePISA* and visual inspection with *Coot* were used to analyze the crystal contacts between psCA3 molecules (Krissinel & Henrick, 2007; Emsley *et al.*, 2010; Table 3). The majority of these interactions were polar in nature, with hydrogen bonds being the most dominant interactions. Interestingly, none of the crystal contact regions involved residues 44–48 (containing the Asp44–Arg46 salt-bridge dyad) which are involved in the pH-controlled opening/closing mechanism of the active site (Fig. 2).

The $P2_12_12$ crystal form diffracted to a resolution of 2.6 Å, with unit-cell parameters a = 88.4, b = 69.4, c = 77.6 Å and an R_{merge} of 15.3%. In this case psCA3 crystallized as a dimer in the asymmetric unit, with eight molecules in the unit cell (Table 3). The refined structure converged to an R_{cryst} of 21.2% and an R_{free} of 27.5%. The data-collection statistics and processing parameters are summarized in Table 1. We also note that an attempt was made to reprocess the reflection data for the $P2_12_12$ form to show that these data preferentially indexed in the primitive orthorhombic rather than the *I*-centered orthorhombic Bravais lattice (*I*222 crystal form). This was confirmed *via* the larger χ^2 error value associated with the *I*-centered lattice after auto-indexing (Table 2).

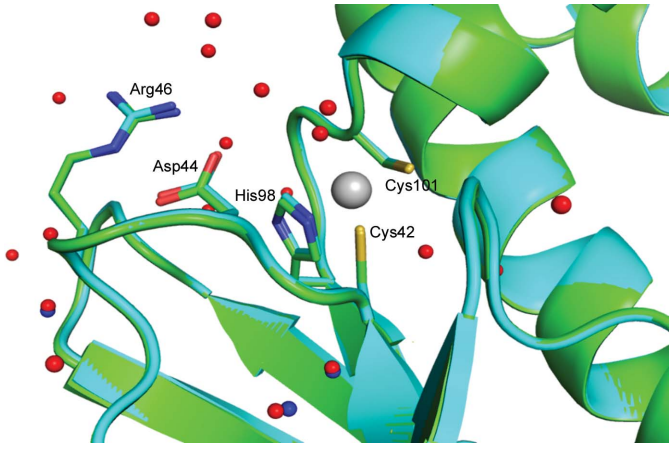

Figure 2
Active-site overlay of psCA3 in space groups *I*222 (cyan) and $P2_12_12$ (light green). Modeled water molecules for the *I*222 structure are shown in red and those for the $P2_12_12$ structure are shown in blue. Note that the Asp44–Arg46 salt-bridge dyad is in the open active-site conformation in both structures. Active-site residues are labeled; the r.m.s.d. between C$^\alpha$ atoms for the two structures is 0.16 Å

Table 4
PDBePISA interface calculations for the *I*222 and $P2_12_12$ crystal forms.

	$P2_12_12$			*I*222		
Interface type	N_{at}†	N_{res}‡	Interface area (Å^2)	N_{at}†	N_{res}‡	Interface area (Å^2)
Dimer	324	77	2892.6	322	77	2908.3
Dimer–dimer	127	33	1244.7	128	34	1245.1
Packing contact I	17	5	188.8	14	5	188.1
Packing contact II	12	5	139.4	11	5	140.1
Packing contact III	12	5	98.2	15	4	124.9
Packing contact IV	6	4	52.3	10	4	68.6
Packing contact V	3	1	37.1	3	1	26.2
Total	501	130	4653.1	503	130	4701.3

† Number of interfacing atoms. ‡ Number of interfacing residues.

Crystal-packing analysis comparison between the two crystal forms revealed no significant differences (Table 4), with the only measurable difference being a modest 48 Å^2 increase in the total interfacial contact area in comparison to the $P2_12_12$ form (Table 4). The arrangements of the psCA3 molecules in each space group are shown in Fig. 1. Despite the protein rigid-body movements in the unit cell there was no significant movement of the 44–48 loop, which is the enzyme-functional on/off switch (Fig. 2). Hence, a functional open active-site configuration with the conserved Asp–Arg dyad was observed in both crystal forms. Overall, the $P2_12_12$ psCA3 structure was very similar to that observed in the *I*222 crystal form (PDB entry 4rxy), with the r.m.s.d. for C$^\alpha$ atoms of chain *A* being 0.16 Å calculated over 204 (of 209) residues. The majority of the stabilization is most likely to be attributable to solvent-mediated inter-protein packing hydrogen bonds (implied by the number of ordered water molecules), which were not observed in the $P2_12_12$ form. This protein/solvent

rearrangement is presumably induced during the cryo-annealing cycling.

Acknowledgements

The authors would like to thank the UF Center for Structural Biology for support of the X-ray facility. We would also like to thank the MacCHESS staff for their help during X-ray diffraction data collection at the Cornell High Energy Synchrotron (CHESS) Facility, Ithaca. CHESS is supported by the NSF and NIH/NIGMS *via* NSF award DMR-1332208, and the MacCHESS resource is supported by NIGMS award GM-103485. This manuscript has been authored by UT-Battelle LLC under DOE Contract No. DE-AC05-00OR22725 with the US Department of Energy. The publisher, by accepting the article, acknowledges that the US Government retains a non-exclusive, paid-up, irrevocable, worldwide license to publish or reproduce the published form of this manuscript, or allow others to do so, for US Government purposes.

References

Adams, P. D. *et al.* (2010). *Acta Cryst.* D**66**, 213–221.
Chen, V. B., Arendall, W. B., Headd, J. J., Keedy, D. A., Immormino, R. M., Kapral, G. J., Murray, L. W., Richardson, J. S. & Richardson, D. C. (2010). *Acta Cryst.* D**66**, 12–21.
Cosier, J. & Glazer, A. M. (1986). *J. Appl. Cryst.* **19**, 105–107.
Covarrubias, A. S., Bergfors, T., Jones, T. A. & Högbom, M. (2006). *J. Biol. Chem.* **281**, 4993–4999.
Covarrubias, A. S., Larsson, A. M., Högbom, M., Lindberg, J., Bergfors, T., Björkelid, C., Mowbray, S. L., Unge, T. & Jones, T. A. (2005). *J. Biol. Chem.* **280**, 18782–18789.
Cronk, J. D., Endrizzi, J. A., Cronk, M. R., O'Neill, J. W. & Zhang, K. Y. J. (2001). *Protein Sci.* **10**, 911–922.
Cronk, J. D., Rowlett, R. S., Zhang, K. Y. J., Tu, C., Endrizzi, J. A., Lee, J., Gareiss, P. C. & Preiss, J. R. (2006). *Biochemistry*, **45**, 4351–4361.
Emsley, P., Lohkamp, B., Scott, W. G. & Cowtan, K. (2010). *Acta Cryst.* D**66**, 486–501.
Frost, S. & McKenna, R. (2013). *Carbonic Anhydrase: Mechanism, Regulation, Links to Disease, and Industrial Applications.* Dordrecht: Springer.
Hanson, B. L., Schall, C. A. & Bunick, G. J. (2003). *J. Struct. Biol.* **142**, 77–87.
Harp, J. M., Timm, D. E. & Bunick, G. J. (1998). *Acta Cryst.* D**54**, 622–628.
Hope, H. (1988). *Acta Cryst.* B**44**, 22–26.
Joseph, P., Turtaut, F., Ouahrani-Bettache, S., Montero, J. L., Nishimori, I., Minakuchi, T., Vullo, D., Scozzafava, A., Köhler, S., Winum, J. Y. & Supuran, C. T. (2010). *J. Med. Chem.* **53**, 2277–2285.
Juers, D. H. & Matthews, B. W. (2004). *Acta Cryst.* D**60**, 412–421.
Kriminski, S., Caylor, C. L., Nonato, M. C., Finkelstein, K. D. & Thorne, R. E. (2002). *Acta Cryst.* D**58**, 459–471.
Krissinel, E. & Henrick, K. (2007). *J. Mol. Biol.* **372**, 774–797.
Lotlikar, S. R., Hnatusko, S., Dickenson, N. E., Choudhari, S. P., Picking, W. L. & Patrauchan, M. A. (2013). *Microbiology*, **159**, 1748–1759.
Oliver, A., Cantón, R., Campo, P., Baquero, F. & Blázquez, J. (2000). *Science*, **288**, 1251–1254.
Otwinowski, Z. & Minor, W. (1997). *Methods Enzymol.* **276**, 307–326.
Pellicane, G., Smith, G. & Sarkisov, L. (2008). *Phys. Rev. Lett.* **101**, 248102.
Pinard, M. A., Lotlikar, S. R., Boone, C. D., Vullo, D., Supuran, C. T., Patrauchan, M. A. & McKenna, R. (2015). *Bioorg. Med. Chem.* **23**, 4831–4838.
Pinard, M., Lotlikar, S., Patrauchan, M. & McKenna, R. (2013). *Acta Cryst.* F**69**, 891–894.
Reyes, M. P. & Lerner, A. M. (1983). *Rev. Infect. Dis.* **5**, 314–321.
Stover, C. K. *et al.* (2000). *Nature (London)*, **406**, 959–964.
Tripp, B. C., Smith, K. & Ferry, J. G. (2001). *J. Biol. Chem.* **276**, 48615–48618.
Yeh, J. I. & Hol, W. G. J. (1998). *Acta Cryst.* D**54**, 479–480.